Canadian Chemical Transactions Year 2015 | Volume 3 | Issue 2 | Page 225-233

Research Article

DOI:10.13179/canchemtrans.2015.03.02.0186

Influence of the Crystal Phase of Magnesium Phosphates Catalysts on the Skeletal Isomerization of 3,3-dimethylbut-1-ene

M. Sadiq[1*], M. Abdennouri[1], N. Barka[1], M. Baalala[2], C. Lamonier[3], M. Bensitel[2]

[1]*Univ. Hassan 1, Laboratoire des Sciences des Matériaux, des Milieux et de la Modélisation (LS3M), BP.145, 25000 Khouribga, Maroc.*
[2]*Laboratoire de Catalyse et Corrosion des Matériaux, Université Chouaib Doukkali, Faculté des Sciences, BP.20, El Jadida 24000, Maroc.*
[3]*Unité de Catalyse et Chimie du Solide, Université de Lille 1, UMR.CNRS.8181, 59650 Villeneuve d'Ascq, France.*

[*]*Corresponding Author: Email: sadiqmhamed@hotmail.com Tel.: +212 666 24 81 96; Fax: +212 523 49 03 54*

Received: *March 23, 2015* ***Revised:*** *May 12, 2015* ***Accepted:*** *May 20, 2015* ***Published:*** *May 21 2015*

Abstract: The nature of the precipitating agent strongly influences the synthesis of magnesium phosphate. Ortho– and pyro–phosphate can be obtained with the use of NaOH and NH_4OH, respectively. Both solids obtained were investigated as synthesized or after calcinations by various physico–chemical techniques such as X–ray diffraction (XRD), diffuse reflectance infrared spectroscopy (DRIFT). The compounds calcined at 773 K have been further characterized by ^{31}P MAS–NMR spectroscopy.
The skeletal isomerisation of 3,3-dimethylbut-1-ene (33DMB1) over MgP and MgPP catalysts is a first order reaction. The catalytic activity increases with the reaction temperature from 493 to 653 K for both solids. It is affected by the crystal phase of magnesium phosphate. The magnesium pyrophosphate (MgPP) catalyst is more active than magnesium orthophosphate (MgP) catalyst in this temperature range.

Keywords: Magnesium phosphate; XRD; ^{31}P MAS–NMR; FT-IR; isomerization of 3,3-dimethylbut-1-ene (33DMB1)

1. INTRODUCTION

Magnesium phosphates have many important applications. They are used as bonding in refractories and mortars, as rapid–setting cements, and in various glasses [1], as biocompatible materials [2]. They play also an important role in catalysis, since they have found use in organic processes where acid–basic surface properties are required [3–5]. Acid–base and redox properties are among important types of surface chemical properties of metal orthophosphates catalysts. The textural and acid–base properties of the catalysts depend on preparation method, concentration of promoting elements; source of phosphate ion and treatment temperature [6–9]. Characterization of crystalline phosphate is often determined using diffraction techniques [3–5]. In the recent years [10,11], it was shown that high–

resolution solid state NMR spectroscopy could also be used successfully to examine such phosphate materials.

A number of metal phosphates have been used as heterogeneous catalysts for various organic processes in recent years, among them, skeletal isomerisation of 3,3-dimethyl-1-butene [12], oxidation of alcohol [13], dehydration of alcohol [14]. Aramendia et al. [15] studied the effect of Na_2CO_3 impregnation on the activity of $Mg_3(PO_4)_2$ in the dehydration 2-hexanol, and shown that the acidity of $Mg_3(PO_4)_2$ decreases after addition of Na_2CO_3. Sokolowskii et al. [3] studied the oxidative transformation of methane on magnesium–phosphorus catalyst and proved the acidity resulting from P on selectivity from dimerization to oxidation. Aramendia et al. [16] have studied an influence of the composition of magnesium phosphate catalysts on the transformation of 2-hexanol. The dehydration–dehydrogenation of alcohols is a model reaction for the acid–base properties of these solid catalysts [17]. In our previous work, we studied the surface acid–base properties by adsorption of specific probe molecules, such as pyridine and 2,6-dimethylpyridine (lutidine), on pure and supported MgP, followed by in situ FT-IR spectroscopy [18]. In that sense, we examined the effect of CoO-MoO_3 impregnation on the activity of amorphous magnesium phosphate in the 3,3-dimethylbut-1-ene (33DMB1) skeletal isomerisation. The results show that the catalytic behaviour of the supported catalysts differs from that of support MgP. We observed at high reaction temperature, the deactivation of CoO-MoO_3/MgP catalysts by deposition of coke contrary to pure MgP.

The 3,3-dimethylbut-1-ene skeletal isomerization has been studied on various metal oxides [19–20] and phosphates [21,12] and supported phosphates [18] and thus, it becomes a model reaction with a mechanism involving secondary carbenium ions on Brônsted sites [19,20].

The skeletal isomerization of 3,3-dimethylbut-1-ene (33DMB1) with the reaction scheme (Figure 1), is relatively simple with only two main products: 2,3-dimethylbut-1-ene (23DMB1) and 2,3-dimethylbut-2-ene (23DMB2). Other weaker products appear at higher temperatures (> 573K). These products are attributed to methylpentenes [19]. The slow step of the reaction is probably the isomerization of the carbocation intermediate through the methyl group migration.

The present work reports on the synthesis of magnesium orthophosphate and magnesium pyrophosphate by varying the nature of the precipitating agent. So, both solids were characterized and tested as catalysts for the skeletal isomerisation 3,3-dimethylbut-1-ene. This reaction allows us to evaluate the Brönsted and Lewis acid sites of these solids.

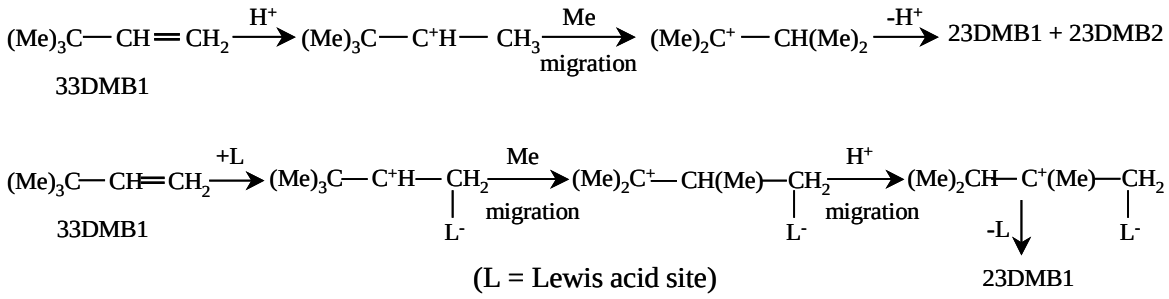

Figure 1. 3,3-dimethylbut-1-ene isomerization scheme.

2. EXPERIMENTAL

2.1. Solid synthesis

Magnesium orthophosphate (MgP) or pyrophosphate (MgPP) were synthesised using the following procedure: a solution containing 40 g of $Mg(NO_3)_2.6H_2O$ and 7.08 cm^3 of H_3PO_4 (purity 85 %)

in 100 cm^3 of distilled water was prepared, the melange was kept in an ice bath. The solution being maintained under stirring, the precipitating agent NaOH (0.4 mol L^{-1}) or NH_4OH (2 mol L^{-1}) was then added dropwise up to pH 9, leading to MgP and MgPP solids respectively. The obtained gel was kept for 24 hours under ambient conditions. It was then filtered, and air–dried at 353 K.

2.2. Characterization techniques

2.2.1. X–ray diffraction analysis

High temperature powder X–ray diffraction (XRD) measurements were recorded on a Siemens D5000 diffractometer using CuK_α radiation. The patterns were recorded with a step of 0.0145° using a counting time 0.2 s per step over the 2θ range from 10° to 80°.

2.2.2. ^{31}P MAS–NMR Spectroscopy

Solid–state ^{31}P NMR spectra were recorded on a Bruker BioSpin GmbH–400 spectrometer at 161.97 MHz, at room temperature. The excitation pulse and recycle time for ^{31}P NMR were 2.5 µs (π/2 pulse) and 3 s (300 scans), respectively. ^{31}P shift was determined in comparison to an 85% H_3PO_4 solution.

2.2.3. IR spectroscopy

Diffuse reflectance infrared spectra for the synthesized solids were recorded from 4000 to 400 cm^{-1} on a Nicolet 460 spectrophotometer at a resolution of 4 cm^{-1}. An overall 128 scans were collected. Samples were prepared by mixing 1 mg of powdered solid with 150 mg of KBr.

2.2.4. Catalytic test

Isomerization of 3,3-dimethylbut-1-ene (33DMB1) was carried out in a fixed–bed type reactor with a continuous flow system at atmospheric pressure. The reactant, 33DMB1 (21.2 kPa), was diluted in nitrogen by bubbling the gas through the liquid reactant in saturator maintained at 273 K. The 33DMB1 isomerization was performed at a temperature between 493 and 653 K. The products were analysed by on line gas chromatography (FID) using a capillary Squalane column (100 m, 0,26 mm id) maintained at 313 K.

The rate constant (mol.h^{-1}.kg^{-1} bar^{-1}) was calculated after each analysis by the form:

$$K(T) = -Ln(1-X)\frac{F_0}{P^0 W}$$

where X is the conversion, P^0 the pressure, F_0 the molar flow rate of 33DMB1 and W (60 mg) the catalyst weight that is previously calcined at 773 K during 3h and sifted through 0.2–0.5 mm.

3. RESULTS AND DISCUSSION

3.1. XRD Results

Figure 2 shows the evolution of the XRD patterns of the dried precipited MgP solid calcined at different temperatures. The uncalcined MgP solid exhibits broad diffraction lines corresponding to $Mg_3(PO_4)_2.5H_2O$ (JCPDS 35-0329), and some low intense diffraction lines that have been assigned to $Mg_3(PO_4)_2.8H_2O$ (JCPDS 33-0877). The XRD diagram showed that the sample was partly amorphous when treated at 473 K and it becomes completely amorphous from 573 K up to 873 K. Beyond 973 K, a crystalline material could be clearly evidenced that corresponds to $Mg_3(PO_4)_2$ (JCPDS 75-1491).

Progressively with the increase in temperature, diffraction lines of the magnesium orthophosphate sharpen indicating a better crystallisation of $Mg_3(PO_4)_2$.

Figure 3 shows the evolution of the XRD patterns of the dried precipited MgPP solid, obtained with the use of NH_4OH, calcined at different temperatures. In the diffraction pattern of the uncalcined solid, the most intense diffraction peaks are attributed to the Dittmarite phase, syn–$NH_4MgPO_4.H_2O$ (JCPDS 36-1491), whereas few weaker peaks are assigned to the $Mg_2P_2O_7$ phase. In the temperature range 373–773 K, the solid $NH_4MgPO_4.H_2O$ was found to be amorphous. Above 773 K, the solid crystallises in an α–$Mg_2P_2O_7$ phase. Parameters of the various magnesium phosphate crystalline phases are reported in our previous work [7].

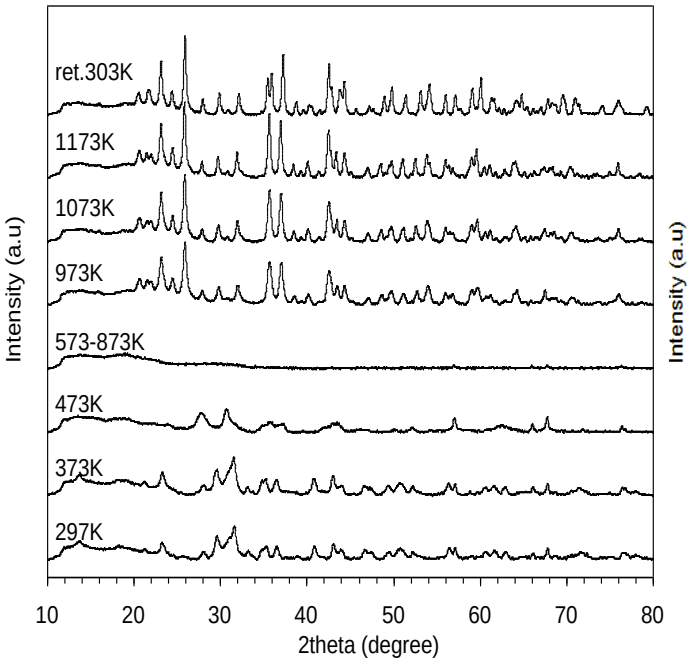

Figure 2. Evolution of the MgP XRD patterns with the temperature treatment.

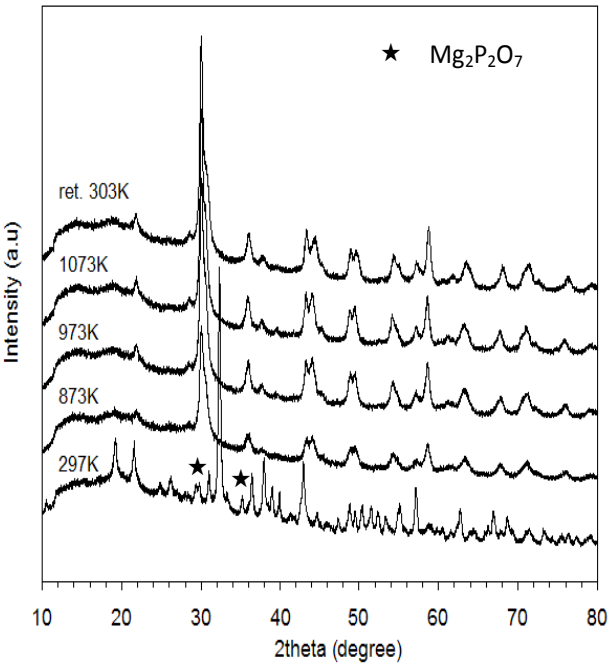

Figure 3. Evolution of the MgPP XRD patterns with the temperature treatment.

3.2. ^{31}P NMR Spectroscopy

Figure 4 shows the ^{31}P MAS NMR spectra for solid MgP and MgPP calcined at 773 K.. At this temperature, the MgP solid is amorphous as we have seen from XRD diffraction. The spectrum for MgP consists of a single component at 0.42 ppm, indicating the presence in this sample of a single type of ^{31}P nuclei, corresponding to the amorphous magnesium orthophosphate $Mg_3(PO_4)_2$. The spectrum for MgPP exhibits three distinct signals, two signals at –18.62 ppm and –11.81 ppm are assigned to an amorphous α–$Mg_2P_2O_7$ phase that contains two crystallographically non–equivalent Q^1 units linked together to an $(P_2O_7)^{4-}$ anion [22]. The additional peak at –13.39 ppm can be in relation to crystalline α-$Mg_2P_2O_7$ previously evidenced from XRD analysis even at room temperature in the uncalcined sample. In the NMR spectrum the weakest signal at 1.84 ppm can be assigned to ^{31}P atom tetrahedrally coordinated in amorphous magnesium orthophosphate [10].

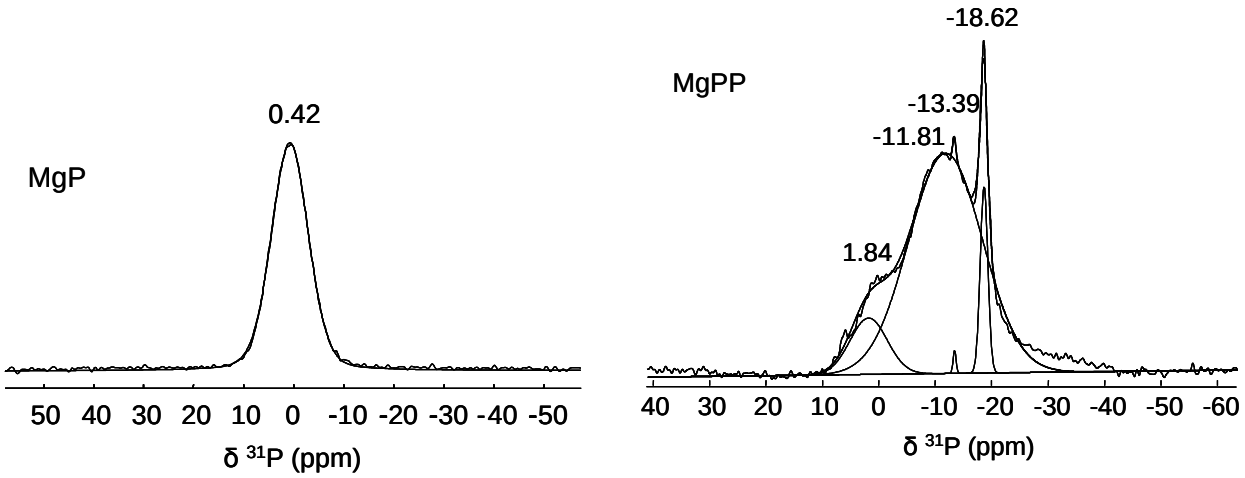

Figure 4. ^{31}P NMR spectra for solids MgP and MgPP calcined at 775K.

3.3. IR spectroscopy

FTIR spectra of MgPP and MgP catalysts calcined at 773 and 973 K are shown in Figure 5. Table 1 summarizes the normal modes of magnesium *ortho*– and *pyro*–phosphates and their attribution according to ref. [23,24] and [25–27], respectively. The IR spectrum of calcined MgP at 773 K shows bands about 1060 cm^{-1} assigned to asymmetric stretching vibration ν_3 of PO_4 phosphate anions, and a band at 574 cm^{-1} that was assigned to out–of–plane bending vibration ν_4 of phosphate. After calcinations at 973 K (figure 5), the spectrum of solid exhibits still the bands for orthophosphates (PO_4^{-3}) ions previously observed, but a band at 982 cm^{-1} clearly appears at high temperature, it is also attributed to symmetric stretching vibration ν_1 of this phosphate PO_4^{3-} [23]. On the other hand, the IR spectra of solid MgPP present the bands, as can be showed in figure 5, due to the presence of pyrophosphate $P_2O_7^{4-}$ species. The P–O vibration band of PO_3 groups appeared at 1105 cm^{-1} that was broadened by two shoulders at 1131 and 1200 cm^{-1}. Those at 990 and 970 cm^{-1} are attributed to the asymmetric stretching vibration ν_{as}(POP) [26]. The IR spectra present also a band at 736 cm^{-1} that is assigned to the symmetric stretching vibration ν_s(POP) bridge, as reported elsewhere [26,27]. The bands around 400–600 cm^{-1} were assigned to the deformation and rocking modes of PO_3 groups (table 1). In the IR spectra of MgPP (figure 5) the weakest band at 1052 cm^{-1} can be assigned to orthophosphate groups PO_4^{3-} previously evidenced from ^{31}P NMR analysis. Furthermore, the symmetric POP bridge stretching mode (ν_s(POP)) can be used to confirm the presence of the pyrophosphate (P_2O_7) group in the MgPP solid. Indeed, the presence of the symmetric and asymmetric bridge stretching vibration (around 736 cm^{-1}) in the infrared spectra of the compounds within this series can be considered as a proof of a bent POP bridge configuration. This is confirming the result obtained previously by XRD (α–$Mg_2P_2O_7$ phase).

The broad absorption was observed in the 3000–3700 cm^{-1} region could be assigned to OH group vibrations bound by hydrogen bond. A less intense band at 1650 cm^{-1} is attributed to the H–O–H bending movement. Additional shoulder at 640 cm^{-1} can be assigned to free vibration of OH (ν_L(O–H)). After increasing temperature, the characteristic hydroxyl bands decrease in intensity; this suggests that dehydration of close OH groups on the solid surface occurred.

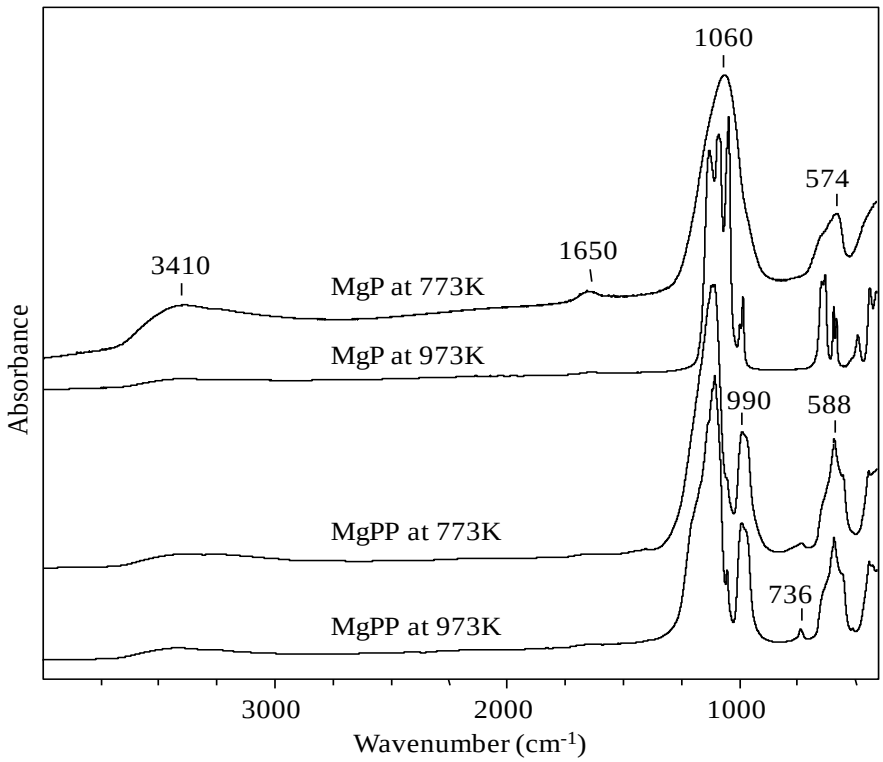

Figure 5: DRIFT spectra for solids MgP and MgPP calcined at 775 and 973 K.

Table 1: FT-IR absorption bands for normal modes of MgPP and MgP with their attribution

Solids	ν (cm^{-1})	normal modes
α-$Mg_2P_2O_7$	About 3410	ν(O-H), H_2O
	1636	δ(H_2O)
	1200 (sh), 1131 (sh), 1105	$\nu_{as}(PO_3)$
	1052	$\nu_{as}(PO_4)$
	990, 970	ν_{as}(P-O-P)
	736	ν_s(P-O-P)
	640 (sh)	ν_L(O-H)
	588, 556, 450	δ(PO_3)
$Mg_3(PO_4)_2$	About 3410	ν(O-H), H_2O
	1650	δ(H_2O)
	1122, 1080, 1042	$\nu_3(PO_4)$
	982	$\nu_1(PO_4)$
	640	ν_L(O-H)
	628, 590, 578, 486	$\nu_2(PO_4)$

sh: shoulder

3.4. 33DMB1 isomerization

The 33DMB1 isomerization reaction was performed at a temperature between 493 and 653 K. Figure 6 shown the catalytic activity of MgP and MgPP catalysts for the 33DMB1 isomerization performed at five reaction temperatures, after four hours of reaction. Both catalysts studied are active in

the 33DMB1 isomerization. As seen in Figure 6 the catalytic activity of MgP and MgPP catalysts increases with the temperature reaction increases. Contrary, Sadiq et al. [18] observed after 573 K the deactivation of MgP supported cobalt–molybdenum catalysts by deposition of coke. Moreover, it was found that the MgPP exhibited high catalytic activity in 33DMB1 isomerization than MgP catalyst in this temperature range; this suggests that MgPP has a highest total number of acid sites. Thus, the high acidity of MgPP is due to the simultaneous presence and with strongest number of Lewis acid sites due to the coordination cations and Brônsted acid sites due to the presence of OH groups bonded to phosphorus P atoms. After reaction at 573 K, small quantity of methylpentenes appears as well as their formation requires relatively strong acid sites [12]. In this sense, Bautista et al. [12] showed that the change in 33DMB1 isomerization activity on $AlPO_4$, $CrPO_4$ and $CrPO_4$-$AlPO_4$ catalysts was related to the change in acid characteristics. They confirmed that the catalytic activity of these catalysts correlated well with their surface acidity values obtained through pyridine and 2,6-dimethylpyridine adsorption.

Moreover, the 23DMB2/23DMB1 ratios for both catalysts decreases with the reaction (pre–treatment) temperature increase as seen in Figure 7, we can be attributed to the transformation of protonic sites to Lewis sites with elimination of hydroxyl groups, according to literature [28]. The 23DMB2/23DMB1 ratio was greater for magnesium orthophosphate than magnesium pyrophosphates catalysts at low treatment temperature, that the water is more easily eliminated from magnesium pyrophosphate than from magnesium orthophosphate (figure 7). In all cases, the 33DMB1 isomerization to 2,3-dimethylbut-2-ene (23DMB2) isomer is the predominant reaction and proceeds via an protonation mechanism through secondary carbonium ions catalysed by Brônsted acid sites. It can be seen also that 23DMB2/23DMB1 ratio is of the same value at a reaction temperature >573 K, this imply that the selectivity towards 23DMB2 and 23DMB1 is similar for both catalysts.

The activation energies determined from the Arrhenius plots for 33DMB1 isomerization are also given between 473 and 573 K. Obviously, the highest activation energy was obtained for MgP (74 $kJ.mol^{-1}$), but it decreased to 45 $kJ.mol^{-1}$ for MgPP. It can be presumed that the surface properties are depending on the structure phase of catalysts.

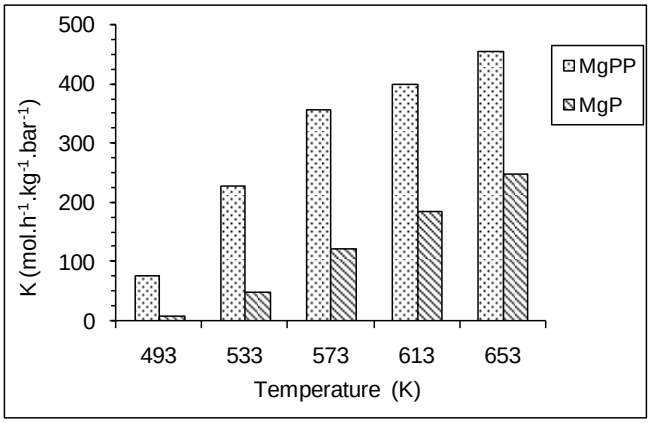

Figure 6. 33DMB1 isomerization as function of the reaction temperature over catalysts calcined at 773K.

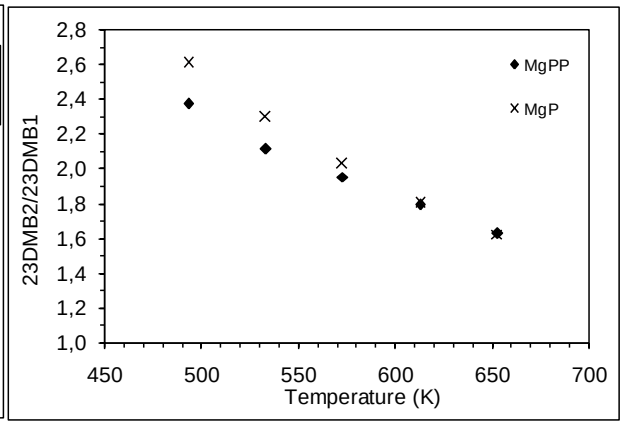

Figure 7. Change of the 23DMB2/23DMB1 ratio versus the reaction temperature.

4. CONCLUSION

The results obtained in this work show that the synthesis of magnesium phosphates depends on the nature of precipitating agent. After a thermal treatment at high temperature, the use of an NaOH solution leads to magnesium orthophosphate whereas the use of an NH_4OH solution produces the magnesium pyrophosphate. MgPP catalyst exhibited higher activity than MgP, in the skeletal isomerization of 3,3-dimethylbut-1-ene. Catalytic activity was strongly influenced by the crystalline structure of magnesium phosphates and thus, magnesium pyrophosphate ($Mg_2P_2O_7$) catalyst obtained by NH_4OH showed the highest activity than magnesium orthophosphate $Mg_3(PO_4)_2$ obtained by NaOH precipitating basic agent. This is due to high number of acidic sites on the surface. Thus, we may conclude that is possible to obtain thermally stable amorphous solids, with a high number of active acid sites, to be used as catalysts, in reaction that need to be carried out on the stronger acid sites.

ACKNOWLEDGEMENT

The authors are grateful to the Comité Mixte Interuniversitaire Franco–Marocain (CMIFM) for financial support through grants MA/02/36 and MA/06/145.

REFERENCES

[1] Fayon, F.; Massiot, D.; Suzuya, K.; Price, D.L. ^{31}P NMR study of magnesium phosphate glasses, *J. Non–Crystalline Solids. 2001, 283, 88–94.*

[2] Nabiyouni, M.; Ren Y.; Bhaduri, S.B. Magnesium substitution in the structure of orthopedic nanoparticles: A comparison between amorphous magnesium phosphates, calcium magnesium phosphates, and hydroxyapatites**,** *Materials Science and Engineering: C, 2015, 52, 11–17.*

[3] Sokolovskii, V.D.; Osipova, Z.G.; Plyasova, L.M.; Davydov, A.A.; Budneva, A.A. Acid–base properties and direction of oxidative transformations of methane on magnesium–phosphorus catalysts, *Appl. Catal. A: Gen. 1993, 101, 15–23.*

[4] Sugiyama, S.; Satomi, K.; Kondo, N.; Shigemoto, N.; Hayashi, H.; Moffat, J.B. Role of surface chlorine species in the oxidative coupling of methane in the presence of tetrachloromethane on magnesium phosphate and sulphate, *J. Mol. Catal. 1994; 93, 53–65.*

[5] Sugiyama, S.; Kondo, N.; Satomi, K.; Hayashi, H.; Moffat, J.B. Effect of tetrachloromethane as a gas–phase additive on the oxidative dehydrogenation of ethane over magnesium phosphate, *J. Mol. Catal. A: Chem. 1995, 95, 35–43.*

[6] Bautista, F.M.; Campelo, J.M.; Garcia, A.; Luna, D.; Marinas, J.M.; Quiros,R.A.; Romero, A.A. Influence of acid-base properties of catalysts in the gas-phase dehydration-dehydrogenation of cyclohexanol on amorphous $AlPO_4$ and several inorganic solids, *Applied Catalysis A: General, 2003, 243, 93–107.*

[7] Sadiq, M.; Bensitel, M.; Lamonier, C.; Leglise, J. Influence of the nature of precipitating basic agent on the synthesis of catalytic magnesium phosphate materials, *Solid State Sciences 2008, 10, 434–437.*

[8] Onoda, H.; Ohta, T.; Tamaki, J.; Kojima, K. Decomposition of trifluoromethane over nickel pyrophosphate catalysts containing metal cation, *Applied Catalysis A, 2005, 288(1-2), 98–103.*

[9] Onoda, H.; Yokouchi, K.; Kojima, K.H. Addition of rare earth cation on formation and properties of various cobalt phosphates, *Materials Science and Engineering: B,* 2005, 116(2), 189–195.

[10] Aramendia, M.A.; Borau, V.; Jiménez, C.; Marinas, J.M.; Romero, F.J.; Ruiz, F.R. XRD and Solid–State NMR Study of Magnesium Oxide–Magnesium Orthophosphate Systems, *J. Solid State Chem. 1998, 135, 96–102.*

[11] Aramendia, M.A.; Borau, V.; Jiménez, C.; Marinas, J.M.; Romero, F.J.; Ruiz, F.R. Characterization by XRD, DRIFT, and MAS NMR Spectroscopies of a $Mg_2P_2O_7$ Catalyst, *J. Colloid and Interface Sci. 1998, 202, 456–461.*

[12] Bautista, F.M.; Campelo, J.M.; Garcia, A.; Luna, D.; Marinas, J.M.; Romero, A.A.; Urbano, M.R. Isomerization of 3,3-dimethyl-1-butene over aluminum and chromium orthophosphates, *React. Kinet. Catal. Lett., N°. 1, 1998, 64, 41–48.*

[13] Li, C.; Kawada, H.; Sun, X.; Xu, H.; Yoneyama, Y.; Tsubaki, N. highly efficient alcohol oxidation on nanoporous VSB-5 nickel phosphate catalyst functionalized by naoh treatment, *ChemCatChem, 2011, 3, 684–689.*
[14] Yaripour, F.; Baghaei, F.; Schmidt, I.; Perregaarad, J. Synthesis of dimethyl ether from methanol over aluminium phosphate and silica-titania catalysts, *Catalysis Communications, 2005 6, 542–549.*
[15] Aramendia, M.A.; Borau, V.; Jiménez, C.; Marinas, J.M.; Romero, F.J.; Urbano, F.J. Effects of Na_2CO_3 impregnation on the catalytic activity of $Mg_3(PO_4)_2$ in the gas-phase conversion of 2-hexanol and the alkylation of aniline with methanol, *J. Coll. and surf. A: Physicochemical and Engineering Aspects, 2000, 170, 51–58.*
[16] Aramendia, M.A.; Borau, V.; Jiménez, C.; Marinas, J.M.; Romero, F.J.; Urbano, F.J. Influence of the structure and composition of magnesium phosphate catalysts on the transformation of 2-hexanol, *J. Mol. Catal. A: Chem. 2002, 182–183, 25–34.*
[17] Aramendia, M.A.; Borau, V.; Jiménez, C.; Marinas, J.M.; Romero, F.J. the Meerwein-Ponndorf–Verley–Oppenauer reaction between 2-hexanol and cyclohexanone on Magnesium phosphate, *Catal. Letters 1999, 58, 53–58.*
[18] Sadiq, M.; Sahibed-dine, A.; Baalala, M.; Nohair, K.; Abdennouri, M.; Bensitel, M.; Lamonier, C.; Leglise, J. Influence of acid–base properties of cobalt–molybdenum catalysts supported on magnesium orthophosphates in isomerization of 3,3-dimethylbut-1-ene, *Arab. J. Chem. 2011, 4, 449–457.*
[19] Martin, D.; Duprez, D. Evaluation of the acid–base surface properties of several oxides and supported metal catalysts by means of model reactions, *J. Mol. Catal. A: chem. 1997, 118, 113–128.*
[20] Haneda, M.; Joubert, E.; Mérézo, J.C.; Duprez, D.; Barbier, J.; Bion, N.; Daturi, M.; Saussey, J.; Lavalley, J.C.; Hamada, H. Surface characterization of alumina–supported catalysts prepared by sol–gel method. Part I. Acid–base properties, *J. Phys. Chem. Chem. Phys. 2001, 3, 1366–1370.*
[21] Florentino, A.; Cartraud, P.; Magnoux, P.; Guisnet, M. Textural, acidic and catalytic properties of niobium phosphate and of niobium oxide: Influence of the pretreatment temperature, *Appl. Catal. A, 1992, 89, 143–153.*
[22] Feike, M.; Graf, R.; Schnell, I.; Jäger, C.; Spiess, H.W. Structure of Crystalline Phosphates from ^{31}P Double–Quantum NMR Spectroscopy, *J. Am. Chem. Soc. 1996, 118, 9631.*
[23] Nakamoto, K. "Infrared and Raman Spectra of Inorganic and Coordination Compounds, Part A, Theory and Applications in Inorganic Chemistry", *Wiley, New York, 2009, 6th Edition.*
[24] Hatert, F.; Rebbouh, L.; Hermann, R.P.; Fransolet, A.-M.; Long, G.J.; Grandjean, F. Crystal chemistry of the hydrothermally synthesized $Na_2(Mn_{1-x}Fe^{2+}_x)_2Fe^{3+}(PO_4)_3$ alluaudite–type solid solution, *American Mineralogist. 2005, 90, 653–662.*
[25] Rulmont, A.; Cahay, R.; liegeois-Duykaerts, M.; Tarte, P. Vibrational spectroscopy of phosphate: Some general correlations between structure and spectra, *Eur.J.Solid State Inorg.Chem. 1991, 28, 207–219.*
[26] Harcharras, H.; Ennaciri, A.; Assaaoudi, H. Vibrational Spectra of Double Diphosphates $M_2SrP_2O_7$ (M=Li,Na,K,Rb,Cs), *Canad.J.Analy. Scien. and Spectr. 2001, 46, 83–88.*
[27] Bih, H.; Saadoune, I.; Ehrenberg, H.; Fuess, H. Crystal structure, magnetic and infrared spectroscopy studies of the $LiCr_yFe_{1-y}P_2O_7$ solid solution, *J. Solid State Chem. 2009, 182, 821–826.*
[28] Burke, P.A.; Ko, E.I., Acidic properties of oxides containing niobia on silica and niobia in silica, *J. Catal. 1991, 129, 38–46.*

The authors declare no conflict of interest

© 2015 By the Authors; Licensee Borderless Science Publishing, Canada. This is an open access article distributed under the terms and conditions of the Creative Commons Attribution license http://creativecommons.org/licenses/by/3.0